Nat Hazards (2017) 85:19–37
DOI 10.1007/s11069-016-2556-x

ORIGINAL PAPER

Targeting flash flood potential areas using remotely sensed data and GIS techniques

Mohamed Abdelkareem[1,2]

Received: 28 June 2016 / Accepted: 24 August 2016 / Published online: 31 August 2016

Abstract Flash floods are the most common type of natural hazards that cause loss of life and massive damage to economic activities. During the last few decades, their impact increased due to rapid urbanization and settlement in downstream areas, which are desirable place for development. Wadi Asyuti, much like other wadis in the Eastern Desert of Egypt, is prone to flash flood problems. Analysis and interpretation of microwave remotely sensed data obtained from the Shuttle Radar Topography Mission (SRTM) and Tropical Rainfall Measuring Mission (TRMM) data using GIS techniques provided information on physical characteristics of catchments and rainfall zones. These data play a crucial role in mapping flash flood potentials and predicting hydrologic conditions in space and time. In order to delineate flash flood potentials in Wadi Asyuti basin, several morphometric parameters that tend to promote higher flood peak and runoff, including drainage characteristics, basin relief, texture, and geometry were computed, ranked, and combined using several approaches. The resulting flash flood potential maps, categorized the sub-basins into five classes, ranging from very low to very high flood potentials. In addition, integrating the spatially distributed drainage density, rainfall intensity, and slope gradient further highlighted areas of potential flooding within the Wadi Asyuti basin. Processing of recent Landsat-8 imagery acquired on March 15, 2014, validated the flood potential maps and offered an opportunity to measure the extent (200–900 m in width) of the flooding zone within the flash flood event on March 9, 2014, as well as revealed vulnerable areas of social and economic activities. These results demonstrated that excessive rainfall intensity in areas of higher topographic relief, steep slope, and drainage density are the major causes of flash floods. Furthermore, integration of remote sensing data and GIS techniques allowed mapping flood-prone areas in a fast and cost-effective to help decision makers in preventing flood hazards in the future.

✉ Mohamed Abdelkareem
mohamed.abdelkareem@sci.svu.edu.eg; mismail@bu.edu

[1] Geology Department, South Valley University, Qena 83523, Egypt

[2] Center for Remote Sensing, Boston University, 725 Commonwealth Ave., Boston, MA 02215-1401, USA

Keywords Remote sensing · GIS · Morphometric analysis · Flash flood hazard

1 Introduction

Remote sensing techniques provided meaningful information that automatically performed spatial analysis using geographic information system (GIS) instead of manual methods. Analysis of remotely sensed data through GIS techniques proved to be fast, accurate, and cost-effective approach in understanding the geologic and geomorphic features. Microwave remote sensing data successfully provided significant qualitative and quantitative information on hydrology, drainage basin analysis, geomorphic/morphotectonic parameters, and geometric and physical characteristics of the terrain (El-Bastawesy et al. 2009; Abdelkareem and El-Baz 2015a, b). Prior to digital images, morphometric analysis was manually performed using topographic maps (Horton 1932; Strahler 1957, 1964; Chorley and Morgan 1962). Remote sensing and GIS techniques allowed extraction of morphometric parameters (Biswas et al. 2014; Lyew-Ayee et al. 2007; Chopra et al. 2005; Rudraiah et al. 2008; Waikar and Nilawar 2014; Somashekar and Ravikumar 2011) and provided valuable information about flash flood potential (Dawod et al. 2011; Abdalla et al. 2014; El-Bastawesy et al. 2009; Youssef et al. 2010).

Strong flash floods cause disruption and destruction of economic and social life. Flash floods are caused by extreme rainfall in a short duration (e.g., Bangira 2013; Bajabaa et al. 2014). Rainfall intensities cause high runoff and flash flooding (Patton and Baker 1976; Syvitski et al. 2009). Such events caused a loss of human lives and massive damage to the infrastructure. Characteristics of catchment areas including relief, geometry, and drainage characteristics provide information on flood potential (Bangira 2013; Bajabaa et al. 2014; Abdalla et al. 2014; Sen et al. 2012; Patton 1988; Gardiner 1990). Despite the arid/hyperarid climate of northeastern Sahara, the elevated areas of the Egyptian deserts, in particular, are subjected to flash flood during heavy sporadic rainfall of winter. This occurs particularly in the highlands of the Red Sea, the northeastern desert of Egypt and Sinai as the high topographic areas receiving the plausible amount of the rainfalls seasons (e.g., Abdelkareem and El-Baz 2015b, c; Abdelkareem et al. 2012a). Lack of vegetation, land cover, infrastructure, and areas of the high slope gradient are significant in controlling, managing, and causing flash flood hazards.

Flood maps are considered an important tool for justifying the impacts of natural hazards (Alkema 2004). Delineating high potential areas of flash floods is of a crucial importance in saving human life and preventing damage to infrastructure including industrial, commercial, and agricultural activities of desert fringes. Using hazard maps allowed for planning several development activities that support leaders and planners in their decisions (Alkema et al. 2001). Therefore, mapping flash flood potential areas are needed for sustainable development plans in new desert fringes. Moreover, it is considered valuable information for leaders and decision makers to prevent flash floods. Although flooding causes damage in areas of high runoff during heavy storms, it represents an important source for recharging alluvial aquifers through porous and fractured rocks in arid regions. Such water resources replenish the groundwater aquifers in areas of good hydraulic conductivity.

The aims of the present study are to (a) understand the geologic and geometric characteristics of the studied Wadi Asyuti basin and its sub-basins based on analysis of the

morphometric parameters using remotely sensed data, and (b) conduct a GIS approaches to delineate the flash flood potential areas.

2 Study area

Wadi Asyuti is a part of the Nile basin in northeastern Sahara (Fig. 1). It is located in the Ma'aza plateau of North Eastern Desert of Egypt, opposite to Asyut Governorate. It lies between longitudes 31°15′ and 32°30′E and latitudes 27° and 27°40′N, occupying an area of about 6000 km^2. It is oriented east–west to drain the Nile basin. It cuts the Ma'aza plateau that is topped by hard massive limestone. The study area is occupied by Cretaceous/Tertiary rocks and Pliocene/Pleistocene deposits. The NW trend is predominant over others and controls the aquifers (Youssef 2008). Based on the average annual (January 1998–November 2013) precipitation about much <10 mm/day (Abdelkareem and El-Baz 2015b), the study area is located in the arid/hyperarid region. Its hyperarid climate makes it an ideal place of remote sensing investigations.

Urban, agricultural, and industrial areas increased due to overpopulation along the narrow Nile Valley, especially, in Asyut city. This pushes the leaders, planners, and decision makers of the local government in terms of seeking new cities for sustainable development. This area represents an important link between southern and northern Egypt. Moreover, several developing projects would be established in the study area, and many farms were reclaimed from the desert fringes. Government leaders and decision makers would support preventing flash flood hazards if they have valuable information and consider that flooding destroys the infrastructure. The Wadi Asyuti area is subjected to many flash floods in the last few decades (1994, 2010, 2014) that destroyed much infrastructure and human life.

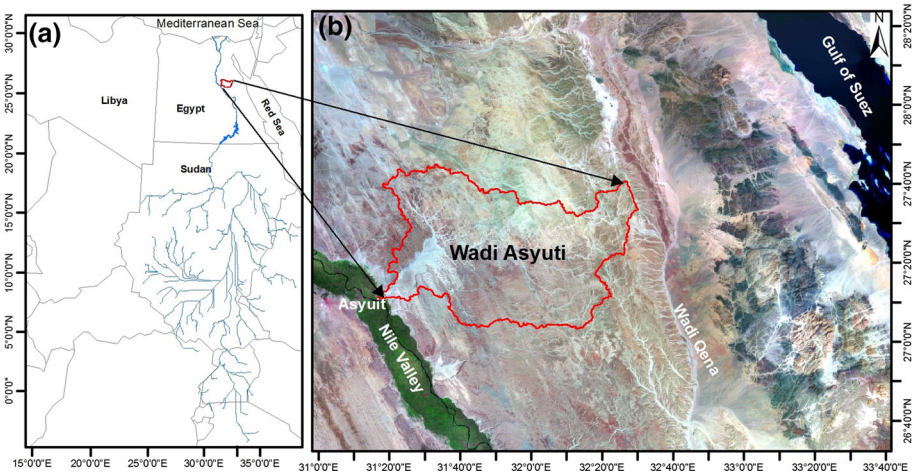

Fig. 1 Egypt's Nile region (**a**) drainage networks of the Nile Basin, the Nile channel is *colored blue*, and the watershed of W. Asyuti is within the polygon marked by *red color*. **b** False *color* 7, 4, 2 (R, G, B) of Landsat ETM+ image overlain by W. Asyuti watershed

3 Data used and methods

Digital elevation models (DEMs) derived from the Shuttle Radar Topography Mission (SRTM) data (~ 90 m cell size) through GIS. The stream networks and the watershed were automatically extracted and performed by applying surface flow routing based on the D8 flow direction algorithm (O'Callaghan and Mark 1984). The extracted streams were automatically classified according to Strahler's (1957, 1964) drainage order. The order indicates the relative position of stream segments in drainage basin networks (Grohmann et al. 2007). The Wadi Asyuti basin was subdivided into 21 sub-basins in order to identify the physical characteristics of the streams and define the most potential areas for flash flooding. The morphometric parameters and its formula which were used in the present study are listed in Table 1.

The DEM of SRTM allowed geomorphic and morphometric analysis and assured satisfactory results in comparison with other topographic maps in a fast and inexpensive fashion (Grohmann et al. 2007; Abdelkareem and El-Baz 2015a). These data allow a quantitative description of basin hydrology based on statistical analysis of morphometric parameters. These parameters include area (km^2), the basin perimeter (km), stream order, bifurcation ratio, drainage density, stream frequency, stream length ratio, infiltration number, basin relief, and basin slope. These parameters were calculated to describe the drainage basin characteristics that reflect the hydrologic conditions and predicting areas of flood hazards are listed in Table 1. Moreover, they reflect the surface and subsurface geology and structures of the basin. In addition to morphometric analysis, microwave data present valuable information of climate that prevails in the area.

A Landsat-8 scene of the downstream area (March 15, 2014) was acquired using the USGS website. It was classified to derive the land cover. This classification was performed after transforming the image using NDVI into vegetated and non-vegetated areas. Using GIS, the vegetated areas, water bodies, and most recent flood zones were extracted based on their reflectance signatures to validate the potential flooding model.

4 Results and discussion

4.1 Analysis of morphometric parameters

The results of SRTM DEM show significant variations in topography that range from 53 (downstream) to 877 m (asl) (upstream). The catchment area is located in the northeastern part that represents the maximum elevation of the tilted plateau (Fig. 2). The topographic break is clearly obvious in the downstream section. We note that the topographic regime of the downstream of about 10 km width and length 40 km of the main channel dramatically changed to the narrower upstream tributaries. Another significant interest in topography is the changes from the east-to-west gradient (Fig. 2), revealing a dominant westerly flow.

The morphometric analysis using remotely sensed data through GIS provided quantitative information of the basin. The perimeter (P) of Wadi Asyuti basin is about 531 km that outlined area (A) of about 6000 km^2. The length (L_b) of the Wadi Asyuti basin is about 129 km from downstream to upstream. The area (A) of the studied sub-basins ranges from 128 to 855.6 Sq km, perimeter 85.05–228.07 km, and the length range from 19.33 to 46.967 km.

Table 1 Morphometric parameters and the expressed formula adopted in the present study

No.	Parameter	Symbol/formula	References
Morphometric parameters			
A	Drainage network		
1	Stream order (u)	u	Strahler (1957, 1964)
2	Stream no. (N_u)	$N_u = N_1 + N_2 + \cdots + N_n$	Horton (1945)
3	Stream length (L_u)	$L_u = L_1 + L_2 + \cdots + L_n$	Strahler (1964)
4	Bifurcation ratio (R_b)	$R_b = N_u/N_u + 1$	Schumn (1956), Strahler (1964)
B	Basin geometry		
1	Basin length (km)	L_b = The longest in the basin in which are end being the mouth	Gregory and Walling (1973)
2	Basin width (km)	W_b = Largest horizontal distance between 2 points, nearly perpendicular to L_b	
3	Area (km)	A	Schumn (1956)
4	Perimeter (km)	P	Schumn (1956)
5	Form factor	$R_f = A/(L_b)^2$	Horton (1932)
6	Elongation ratio	$L_e = 2\sqrt{(A/\pi)}/L_b$	Schumn (1956)
7	Texture ratio	$T = N_1/P$	Schumn (1956)
8	Circulatory ratio	$R_c = 4\pi A/P^2$	Miller (1953)
C	Drainage texture analysis		
1	Stream frequency	$F_s = \sum N_u/A$	Horton (1932, 1945)
2	Drainage density (km/km^2)	$D_d = \sum L_u/A$	Horton (1932, 1945)
3	Constant channel maintenance (C)	$C = 1/D_d$	Schumn (1956)
4	Infiltration number	$I_f = D_d \times F_s$	Faniran (1968)
5	Length of overland flow (km)	$L_g = 1/(2D_d)$	Horton (1945)
D	Relief characterizes		
1	Basin relief (km)	$B_h = Z_x – Z_m$	Strahler (1952, 1957)
2	Relief (gradient) ratio or Basin slope (km)	$R_h = B_h/L_b$	Schumn (1956)
3	Ruggedness number	$R_n = B_h \times D_d$	Schumn (1956), Melton (1957), Strahler (1964)

Wadi Asyuti of seventh-order drainage pattern according to Strahler (1957, 1964). The stream networks are mostly of rectangular drainage geometry. The NW streams parallel each other and cut the main channel of the wadi. This reflects the role of the NW trend on shaping the streams that followed the structural elements as most tributaries running in NW direction are perpendicular to the main channel.

The bifurcation ratio (R_b) of the studied sub-basins ranges from 3.54 to 5.045 with a mean value of 4.295 (Table 2). This seems to be that the geological structures have less effect on the drainage system (e.g., Nageswara Rao et al. 2010). Strahler (1964) revealed that the values of bifurcation ratios, in general, ranging from 3.0 to 5.0 are found to be associated with drainage of little or no geologic structure distortion. This is because the

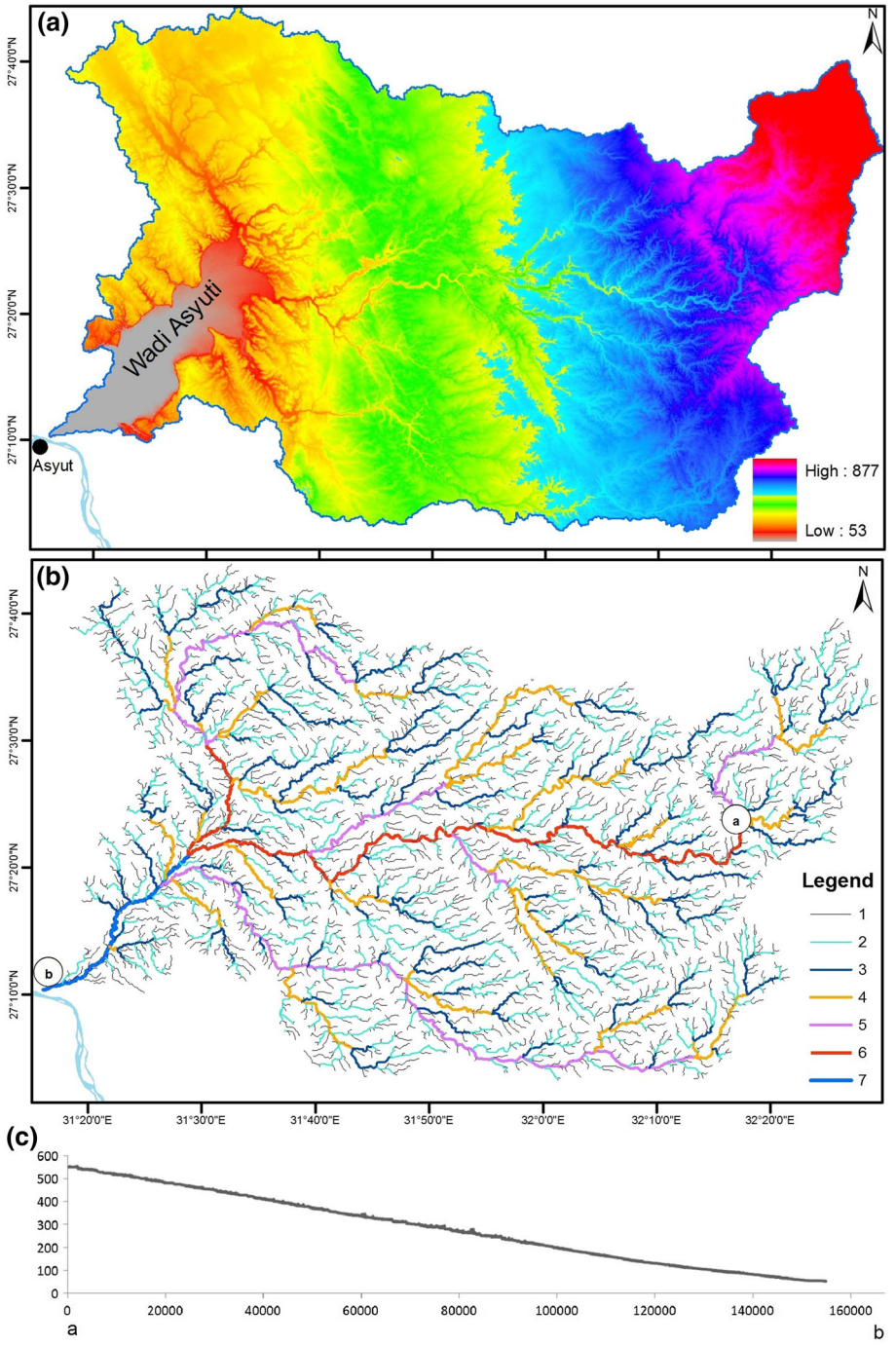

Fig. 2 Topographic views of the study area **a** digital elevation model (DEM) based on SRTM showing the variations on elevation in the area, **b** stream order of the W. Asyuti, **c** longitudinal profile along transect **a**–**b** of the main stream of W. Asyuti

higher values reveal structural control on the development of the drainage system (Strahler 1964; Biswas et al. 2014) and structural disturbances have conducted in the basin (e.g., Withanage et al. 2014). Focusing on runoff and flash floods, the higher R_b value (e.g., sub-basins# 16, 12, 13, 8, and 5) gives an indication of a slow surface flow and lower flood risk (Withanage et al. 2014; Chorley et al. 1957), which allowed water to infiltrate into alluvial aquifers and decrease the runoff and flash flood (i.e., Abdalla et al. 2014). This higher value of R_b, along with elongated shape, tends to reduce the risk of flooding (e.g., Withanage et al. 2014). However, the lower values, especially in areas of high relief, maximize the efficient of flood potentials (e.g., sub-basins 9, 1, and 4; Fig. 3a).

Concerning the geometric characteristics (Table 2) and shape of the studied sub-basins, the computed elongation ratio (R_e), form factor (R_f), and circularity ratio (R_c) revealed that the basin is not circular in nature but has elongated geometry. The R_e of the sub-basins ranges from 0.430 (sub-basin #3) to 0.840 (sub-basin #20), revealing that they are oval to more elongated (Fig. 3b). This based on the elongation ratio, in general, classifying into circular (0.9–1.0), oval (0.8–0.9), less elongated (0.7–0.8), elongated (0.5–0.7), and more elongated (<0.5) (Schumn 1956). Moreover, the mean value of form factor (R_f) (Horton 1932) is about 0.35 that ranges from 0.15 to 0.55, revealing the elongated shape (Fig. 3c). This is because values of form factor (R_f) would always >0.7584 for a circular basin the values above that are circular geometry. Because the form factor (R_f) represents a quantitative illustration of the drainage basin outline shape. Therefore, the smaller the value, the more elongated will be the basin. The form factor (R_f) values are strongly positive with the computed elongation ratio (R_e) values. For further clarification of the basin shape and geometry, we computed the circularity ratio (R_c) based on the Miller concept (1953). The circularity ratio (R_c) of the studied sub-basins (Fig. 3d) ranges from 0.130 (sub-basin #12) to 0.345 (sub-basin #4) with a mean 0.237 indicating no circular shape (circular when $R_c = 1$) but elongated. This geometry suggests that the estimated time for the flow to accumulate in the main channel is more than that required in the circular sub-basins (Miller 1953).

The aforementioned results clarify that a significant positive relationship exists between R_e, R_f, and R_c. These morphometric parameters mostly showed an oval, elongated, and more elongated shape that attributed a longer travel time than circular sub-basins. This reflects low risk of flood, low discharge of runoff, and chances for high infiltration capacity (e.g., Miller 1953; Singh and Singh 1997; Waugh 1995). Therefore, these sub-basins are easier to be controlled and managed than that from the circular one as the circular sub-basins are more effective in the discharge of runoff. Moreover, revealing high chance for infiltration into groundwater table in areas of large thickness of alluvial deposits that recharged during heavy storms.

In addition to the previous analysis, understanding the population and spatial distribution of the streams (texture) are of crucial importance on revealing the ambiguity of hydrologic conditions and predicting areas of flood potential. Thus, we further analyzed the texture ratio, stream frequency, drainage density and length of overland flow (Fig. 3; Table 2). The texture ratio (T) is calculated by the number of stream segments of the first order per perimeter (P) of that area. In the present study, the drainage texture (Fig. 3e) of the studied sub-basins ranges from 2.32 (sub-basin #14) to 7.08 (sub-basin #21) with mean value of about 4.7, which seems to be a moderate drainage texture based on the Smith (1950) classification (i.e., very coarse <2, coarse 2–4, moderate 4–6, fine 6–8, and very fine >8).

The stream frequency (Fs) (Horton 1932, 1945) of the studied sub-basins ranges from 2.266 (sub-basin #6) to 2.760 (sub-basin #18) with a mean value of 2.71, reflecting a low

Table 2 Results of the morphometric parameters of Wadi Asyuti sub-basins, (U) order, (A) area, (P) perimeter, (L_b) basin length, (W_b) basin width, (R_b) mean bifurcation ratio, (R_e) Elongation ratio, (R_f) form factor, (R_c) circularity ratio, (T) texture ratio, (F_s) stream frequency, (D_d) drainage density, (L_g) length of overland flow, (I_f) infiltration number, (B_h) basin relief, (R_h) relief ratio, (R_n) ruggedness no

Basin#	U	N_u	L_u	A	P	L_b	W_b	R_b	R_e	R_f	R_c	T	F_s	D_d	L_g	I_f	B_h	R_h	R_n
1	6	620	477.9	247.93	136.72	31.24	12.27	3.61	0.57	0.25	0.17	3.57	2.5	1.93	0.26	4.82	0.194	0.006	0.37
2	5	318	250.63	127.33	85.06	21.84	8.88	4.13	0.58	0.27	0.22	2.95	2.5	1.97	0.25	4.92	0.16	0.007	0.315
3	5	454	368.48	196.57	133.41	35.12	9.53	4.365	0.43	0.15	0.14	2.68	2.31	1.87	0.27	4.33	0.194	0.005	0.36
4	6	509	405.9	214.88	88.52	22.94	14.16	3.62	0.72	0.41	0.34	4.59	2.37	1.89	0.26	4.47	0.169	0.007	0.32
5	5	534	434.17	227.85	110.26	26.7	14.85	4.6	0.6	0.28	0.24	3.93	2.34	1.91	0.26	4.47	0.249	0.009	0.47
6	5	290	240.19	128	92.3	22.65	11.63	4.17	0.56	0.25	0.19	2.52	2.266	1.876	0.27	4.25	0.204	0.009	0.38
7	6	762	598.64	308.51	128.84	30.76	15.15	3.91	0.64	0.33	0.23	4.58	2.47	1.94	0.26	4.79	0.244	0.008	0.47
8	5	661	515.74	268.85	149.79	38.94	11.73	4.79	0.475	0.18	0.15	3.465	2.46	1.92	0.26	4.72	0.295	0.008	0.57
9	6	482	390.31	198.63	90.57	19.34	16.03	3.545	0.82	0.53	0.3	4.32	2.43	1.965	0.25	4.77	0.202	0.01	0.4
10	6	861	706.69	347.14	159.87	36.37	19.55	3.91	0.58	0.26	0.17	4.28	2.48	2.036	0.246	5.05	0.321	0.009	0.65
11	6	838	697.6	355.99	157.67	38.19	17.33	3.89	0.56	0.24	0.18	4.21	2.35	1.96	0.26	4.61	0.295	0.008	0.58
12	5	648	523.39	271.15	160.34	42.33	11.35	4.76	0.44	0.15	0.13	3.2	2.39	1.93	0.26	4.61	0.361	0.0085	0.7
13	5	772	665.53	327.72	133.57	34.12	12.92	5.01	0.6	0.28	0.23	4.6	2.36	2.03	0.25	4.78	0.273	0.01	0.73
14	5	300	228.02	118.51	102.54	26.42	10.77	4.25	0.465	0.17	0.14	2.32	2.53	1.92	0.26	4.9	0.216	0.014	0.7
15	6	936	761.19	401.5	142.39	31.05	18.57	3.95	0.73	0.42	0.25	5.27	2.33	1.9	0.26	4.42	0.258	0.01	0.49
16	5	792	665.09	337.68	156.56	41.63	14.37	5.045	0.5	0.195	0.17	4.024	2.345	1.97	0.25	4.62	0.292	0.007	0.575
17	5	413	331.74	168.3	108.05	21.81	11.38	4.25	0.54	0.23	0.18	2.94	2.45	1.97	0.25	4.84	0.125	0.011	0.58
18	5	478	367.4	173.06	112.78	23.99	11.11	4.62	0.62	0.31	0.17	3.25	2.76	2.123	0.236	5.86	0.115	0.005	0.244
19	6	1179	955.79	460.87	200.04	46.97	18.04	4.02	0.52	0.21	0.145	4.64	2.56	2.1	0.24	5.31	0.247	0.005	0.51
20	6	644	570.07	282	130.26	22.66	15.57	3.56	0.84	0.55	0.21	3.85	2.28	2.02	0.25	4.62	0.214	0.011	0.5
21	6	2069	1812.95	855.6	228.07	44.05	37.8	4.4	0.75	0.44	0.21	7.08	2.42	2.12	0.236	5.12	0.31	0.007	0.66

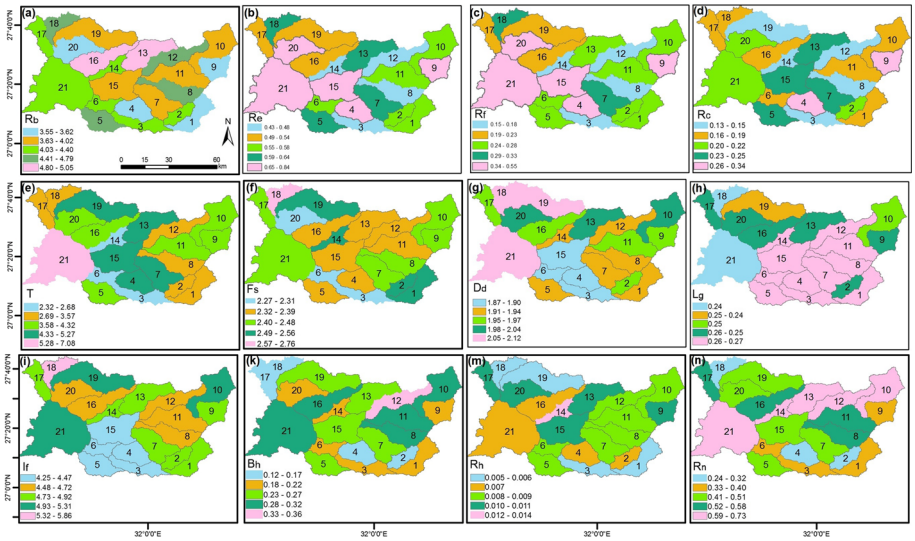

Fig. 3 Morphometric parameters of W. Asyuti **a** Bifurcation ratio (R_b), **b** elongation ratio (R_e), **c** form factor (R_f), **d** circularity ratio (R_c), **e** texture ratio (T), **f** stream frequency (fs), **g** drainage density (D_d), **h** length of overland flow (lg), **i** infiltration number (if), **k** basin relief (B_h), **m** relief ratio (R_h), **n** ruggedness number (R_n)

value (Fig. 3f). As Kale and Guptha (2001) concluded, the F_s value may range from <1 to 6 or even more dependent on the lithology of the basin. Based on the computed values, the sub-basins possess a low relief and almost a flat topography (Horton 1932). Moreover, the closeness of spaces of streams (drainage density, D_d) effect on the accumulated runoff, and higher value accelerate the runoff. The drainage density ranges from 1.870 km/km^2 (sub-basin #3) to 2.123 km/km^2 (sub-basin #18) with mean value of 1.996 km/km^2 (Fig. 3g). Values <1 km/km^2 reflect high permeable deposits; however, in impermeable deposits it increases to 5 km/km^2 (e.g., Withanage et al. 2014). It is noteworthy that the D_d has a positive relationship with the F_s value indicating lowering stream population with respect to decreasing in drainage density (Withanage et al. 2014). To maximize the extracted information of drainage density, we computed the length of overland flow ($lg1/2D_d$, Horton 1945). Based on this analysis (Fig. 3h), it ranges from 0.236 (sub-basin #4) to 0.270 (sub-basin #3) with a mean value of about 0.253. Sub-basins of low value (e.g., sub-basins # 21 and 18) indicate surface water runoff accumulates faster than those of high values (Fig. 3h), revealing high risk. Multiplying both drainage density and stream frequency presents the infiltration number (lf) (Faniran 1968). The studied sub-basins range from 4.250 (sub-basin #6) to 5.860 (sub-basin #18) with a mean value of about 5.055. The relatively higher values reveal higher runoff and low infiltration capacity (Fig. 3i).

Understanding the relief properties of the studied sub-basins provided valuable information on slope and terrain ruggedness that have a direct effect on the flood intensity. This is because increasing slope and ruggedness accelerate the runoff. The total basin relief (B_h) is defined as the difference in elevation between the highest point (Z) of watershed and the lowest point (z) on the valley floor ($B_h = Z - z$) (Strahler 1952, 1957), revealing variability in the elevation of upstream and downstream. Therefore, the Wadi Asyuti basin relief is 0.824 km. Likewise, the studied sub-basins range from 0.115 km (sub-basin #18) to 0.361 km (sub-basin #12; Fig. 3k) with a mean value of about 0.238 km. However, this

value (B_h) divided by basin length (L_b) would present the relief ratio (R_h) which reflects the basin gradient. The relief ratio of Wadi Asyuti is about 0.592, indicating the basin of low slope and relief (Fig. 3m). The relief ratio of the studied sub-basins ranges from 0.005 (sub-basin #16) to 0.014 (sub-basin #14) with a mean value of about 0.0095, reflecting lower values of low relief. To maximize the extracted information of slope and ruggedness, the basin relief (B_h) and drainage density (D_d) are multiplied to compute the ruggedness number (R_n; Table 1). The mean R_n of the studied sub-basins is 0.487. The R_n values (Fig. 3n) of the studied sub-basins range from 0.244 (sub-basin #18) to 0.730 (sub-basin #13). Basins of higher values of R_n reflecting steep slope relative to those of lower values (Strahler 1957, 1964).

4.2 Mapping flash flood potentials

The properties of the morphometric parameters of basins and sub-basins to flood risk have been conducted by many studies (e.g., Schumn 1956; Horton 1945; Marchi et al. 2010; Bangira 2013). The morphometric properties reflect the climate, geology, soil, and runoff properties of the studied basin. Therefore, the flash flood potential areas will be delineated using 12 effective parameters (R_b to R_n) that lished in Table 2. The higher relief ratio (catchment steepness), and drainage density (closeness of streams), the higher flood risk (Horton 1945). Likewise, stream slope and ruggedness characteristics promote the high risk of flood (Patton and Baker 1976) as the high stream gradient and high relief increase the flow velocity. This is because relief ratio describes the total relief to the length and total relief describes the differences between highest and lowest points (e.g., Bangira 2013). However, the drainage density (D_d) is a factor of soil permeability (low D_d reveal higher permeable soil) and relief characteristics.

The geometric characteristics of the basin area are of significant effect on flash flood potential. Areas of higher R_e, R_f, and R_c values tend to have higher runoff and flash flood hazards. This is because the circular basin shape promotes runoff rather than the elongated basin. Moreover, the circular basin reveals high discharge over a short period of time (e.g., Singh and Singh 1997; Schumn 1956; Waugh 1995; Miller 1953; Bangira 2013).

In addition to basin geometry and relief properties, the low bifurcation ratio causes higher flood risk (Bangira 2013; Abdel Ghaffar et al. 2015; Withanage et al. 2014; Chorely et al. 1957; Abdalla et al. 2014).

In the ongoing discussion, we map flood hazards using morphometric parameters using different methods. Moreover, we integrate rainfall data, land cover and terrain characteristics to the extent of the flood zone in the downstream area.

4.2.1 Integration of raster layers

Integrating data were conducted based on assigning different weights to each class in the combined raster layers (e.g., Abdelkareem et al. 2012b). Raster data are built up of cells (pixels) that are arranged in rows and columns. Raster analysis allows combining many input rasters that have the same row and column geometry of the pixels. This approach can be done by preparing raster GIS layers of higher values as drainage density, relief ratio, ruggedness, form factor, elongation ratio, circularity ratio, stream frequency, texture ratio, infiltration number, channel gradient, and lower values of bifurcation ratio and length of overland flow. This operation can be performed by converting multiple rasters to a common measurable scale, assigning a weight to each raster according to its significance to flood potential (Table 3). Subsequently, each GIS layer is divided into five classes as

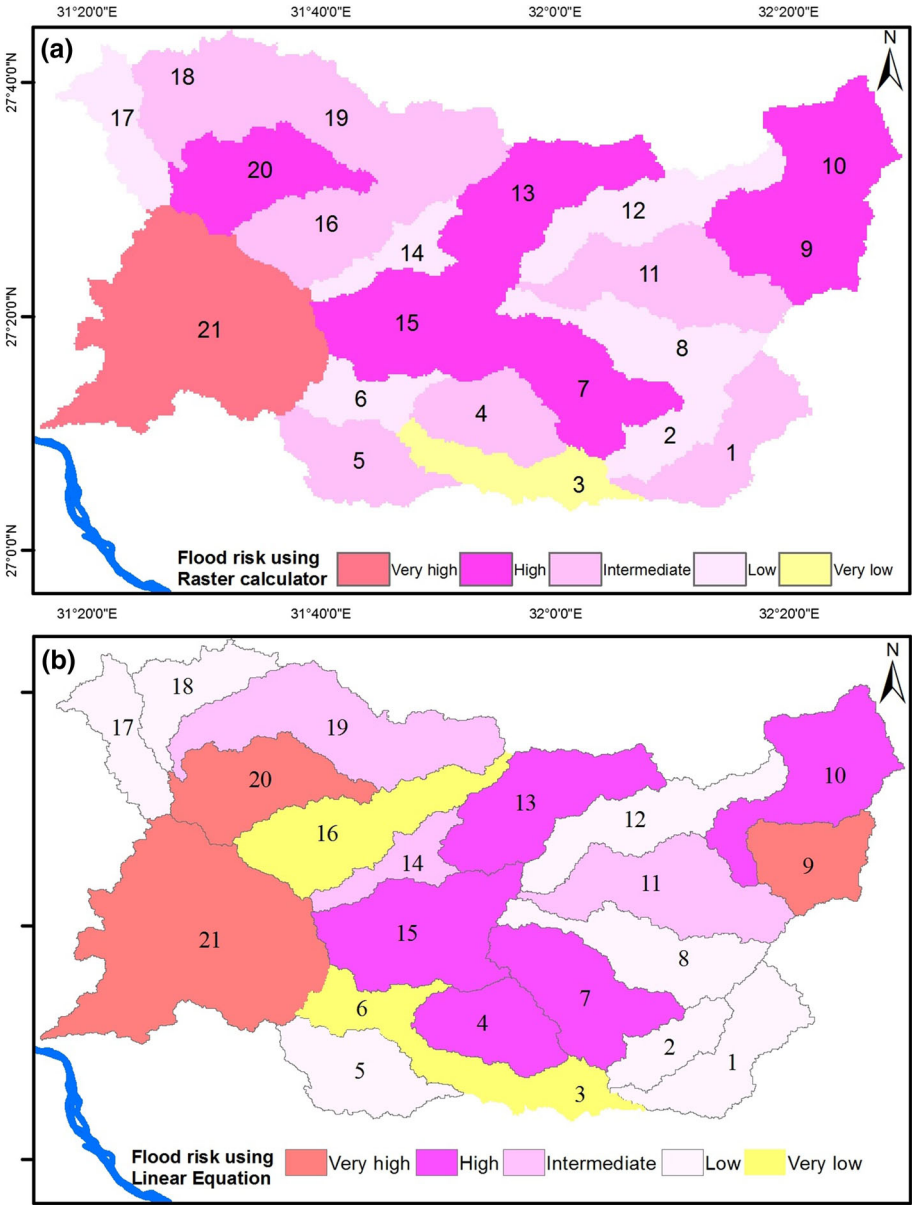

Fig. 4 Flood potential maps **a** flood potential map based on integrated thematic layers, **b** flood potential map based on linear equation (Davis 1975)

shown in Fig. 3a. Sub-basins with high values of runoff were assigned the high weight of 5 and low values have weight of 1 (Table 3). These were integrated using Raster Calculator of ArcGIS software package to highlight areas with factors that promote higher flood peaks and runoff. This hazard map was graded into five categories depending on their significance to cause high and effective runoff. Sub-basins (sub-basins #21, 20, and 10) which

Table 3 Raster layers weights to flood potentials and higher runoff

Factor	Classes	Weight	Factor	Classes	Weight
Bifurcation ratio (R_b)	3.55–3.62	5	Drainage density (D_d)	1.87–1.90	1
	3.63–4.02	4		1.91–1.94	2
	4.03–4.40	3		1.95–1.97	3
	4.41–4.79	2		1.98–2.04	4
	4.80–5.05	1		2.05–2.12	5
Elongation ratio (L_e)	0.43–0.48	1	Length of overland flow (L_g)	0.0–0.24	5
	0.49–0.54	2		0.24–0.25	4
	0.55–0.58	3		0.25	3
	0.59–0.64	4		0.025–0.26	2
	0.65–0.84	5		0.26–0.27	1
Form factor (R_f)	0.15–0.18	1	Infiltration ratio (I_f)	4.25–4.47	1
	0.19–0.23	2		4.48–4.72	2
	0.24–0.28	3		4.73–4.92	3
	0.29–0.33	4		4.93–5.31	4
	0.34–0.55	5		5.32–5.86	5
Circularity ratios (R_c)	0.13–0.15	1	Basin relief (B_h)	0.12–0.17	1
	0.16–0.19	2		0.18–0.22	2
	0.20–0.22	3		0.23–0.27	3
	0.23–0.25	4		0.28–0.32	4
	0.26–0.34	5		0.33–0.36	5
Texture ratio (T)	2.32–2.86	1	Relief ratio (R_h)	0.005–0.006	1
	2.69–3.57	2		0.006–0.007	2
	3.58–4.32	3		0.008–0.009	3
	4.33–5.27	4		0.010–0.011	4
	5.28–7.08	5		0.012–0.014	5
Stream frequency (F_s)	2.27–2.31	1	Ruggedness number (R_n)	0.24–0.32	1
	2.32–2.39	2		0.33–0.40	2
	2.40–2.48	3		0.41–0.51	3
	2.49–2.56	4		0.52–0.58	4
	2.57–2.76	5		0.59–0.73	5

have an extreme probability to flash flood potential are shown in Fig. 4a; however, those of low runoff potential are sub-basins #3, and 6. Most of the higher potential flooding sub-basins occur in the upstream of Wadi Asyuti basin (Fig. 4a).

4.2.2 Using linear equations

We applied linear equations (Davis 1975) for the selected morphometric parameters (Table 4) including, R_e, R_f, R_c, T, F_f, D_d, if, B_h, R_h, R_n, R_b, and L_g. The first ten parameters have a positive relationship with flood hazards; however, lower R_b and L_g values promote runoff and show an inverse relationship. Therefore, the flood potential of each sub-basin was performed by calculation of the intermediate values between the sample points,

Table 4 Hazard degree for morphometric parameters; (15–20) = 1, (20–25) = 2, (25–30) = 3, (30–35) = 4, (35–40) = 5, (40–45) = 6

Basin_No	R_b	R_e	R_f	R_c	T	F_s	D_d	L_g	I_f	B_h	R_h	R_n	$\sum$ of hazard degree	Hazard degree
1	4.827	2.366	2	1.762	2.05	2.833	1.949	2.176	2.416	2.285	1.444	2.037	28.14545	3
2	3.44	2.463	2.2	2.714	1.529	2.833	2.581	3.353	2.665	1.732	1.889	1.584	28.98397	3
3	2.813	1	1	1.19	1.303	1.25	1	1	1.199	2.285	1	1.955	16.99437	1
4	4.8	3.829	3.6	5	2.908	1.75	1.316	2.176	1.547	1.878	1.889	1.626	32.31854	4
5	2.187	2.659	2.3	3.095	2.353	1.5	1.632	2.176	1.547	3.179	2.778	2.86	28.26557	3
6	3.333	2.268	2	2.143	1.168	0.883	1.095	1	1	2.447	2.778	2.119	22.23502	2
7	4.027	3.049	2.8	2.905	2.899	2.583	2.107	2.176	2.342	3.098	2.333	2.86	33.17848	4
8	1.68	1.439	1.3	1.381	1.962	2.5	1.791	2.176	2.168	3.927	2.333	3.683	26.34014	3
9	5	4.805	4.8	4.238	2.681	2.25	2.502	3.353	2.292	2.415	3.222	2.284	39.8413	5
10	4.027	2.463	2.1	1.762	2.647	2.667	3.625	3.824	2.988	4.35	2.778	4.342	37.57026	5
11	4.08	2.268	1.9	1.952	2.588	1.583	2.423	2.176	1.894	3.927	2.333	3.765	30.89164	4
12	1.76	1.098	1	1	1.739	1.917	1.949	2.176	1.894	5	2.556	4.753	26.84186	3
13	1.093	2.659	2.3	2.905	2.916	1.667	3.53	3.353	2.317	3.569	3.222	5	34.52995	4
14	3.12	1.341	1.2	1.19	1	3.083	1.791	2.176	2.615	2.642	5	4.753	29.91253	3
15	3.92	3.927	3.7	3.286	3.479	1.417	1.474	2.176	1.422	3.325	3.222	3.025	34.37346	4
16	1	1.683	1.45	1.762	2.432	1.542	2.581	3.353	1.919	3.878	1.889	3.724	27.21287	3
17	3.12	2.073	1.8	1.952	1.521	2.417	2.581	3.353	2.466	1.163	3.667	3.765	29.87773	3
18	2.133	2.854	2.6	1.762	1.782	5	5	5	5	1	1	1	34.13041	4
19	3.733	1.878	1.6	1.286	2.95	3.333	4.636	4.529	3.634	3.146	1	3.189	34.91497	4
20	4.96	5	5	2.524	2.286	1	3.372	3.353	1.919	2.61	3.667	3.107	38.79668	5
21	2.72	4.122	3.9	2.524	5	2.167	4.953	5	3.161	4.171	1.889	4.424	44.02998	6

considering a straight linear relationship exists between them (e.g., Bajabaa et al. 2014). The hazard degree for the first ten parameters (Table 4) is calculated using equation #1, but R_b and L_g (Table 4) are computed using equation #2. Therefore, the total hazard degree for each sub-basin is listed in Table 3. Equations (2) are used:

$$\text{Hazard degree} = \frac{4(X - X_{\min})}{X_{\max} - X_{\min}} + 1 \quad (1)$$

$$\text{Hazard degree} = \frac{4(X - X_{\max})}{X_{\min} - X_{\max}} + 1 \quad (2)$$

where X represents the value of morphometric parameters to be estimated for flood potentials for each sub-basin; and $X_{\max}$ and $X_{\min}$ represent the maximum and minimum values of the morphometric parameters of all sub-basins, respectively (e.g., Davis 1975; Bajabaa et al. 2014).

Based on the estimated hazard degree, the extreme hazards are recorded in many sub-basins such as sub-basin #21, 9, 20, and 10; however, low hazards in sub-basins 3 and 6 (Table 4; Fig. 4b). The hazard probability potential map was classified into 5 classes based on the quantitative classifier of the GIS. Based on the summation of hazard degree in Table 4, the distribution of hazard degree of the studied sub-basins is shown in Fig. 4b. The main difference between the two methods is depicted in Fig. 4a, b.

4.2.3 Rainfall, floodway, and active streams versus flood potentials

Although the aforementioned methods clearly highlighted the sub-basins of extreme severity, the final output (Fig. 4a, b) still broader and the information is not effective in supporting the leaders and decision makers to take action in reducing flash flood hazards in specific areas of the Wadi that of special interest. For example, the aforementioned potential map considered the entire sub-basin #21 is a dangerous area, but this is incorrect in reality because many areas of this sub-basin are safe. Furthermore, it cannot include all we need to delineate areas which lead to risks. Due to this limitation, we examined several other sources of information to realize how the actual risk area connects to social and economic activities. In addition, these maps are not effective to leaders, decision makers, and end users. Therefore, there is a need to generate complementary information including rainfall data, spatial analysis of slope and drainage density, and land-use/cover data for highlighting potential areas along the streams and define the extent of the flood zone.

Flash flood that have occurred many years back might be of significant importance in understanding the scenarios of the present and future areas of potential flooding. Utilizing remotely sensed rainfall (TRMM) data provide information about spatiotemporal rainfall data and storms. On March 9, 2014, small catchments (sub-basins# 9, 10, 11, and 12) received a high intensity of rainfall precipitation, in particular, the northeastern sub-basins (Fig. 5a). These areas have high spatial variations in topography that results in variations on receiving rainfall. As these catchments received high rainfall anomalies than other catchments, the main channel (W. Asyuti) connected to these sub-basins has to collect much more water than others. Mapping areas of high stream density and steep slope highlighted the hazard areas along that channel (Fig. 5b, c). These areas have the possibilities of flood potentials, because of excessive rainfall precipitation in areas of a steep slope and high relief (Fig. 5a–c) that promote higher runoff and cause massive damage. Moreover, the areas with high rainfall are more prone to flash flooding as match up to those

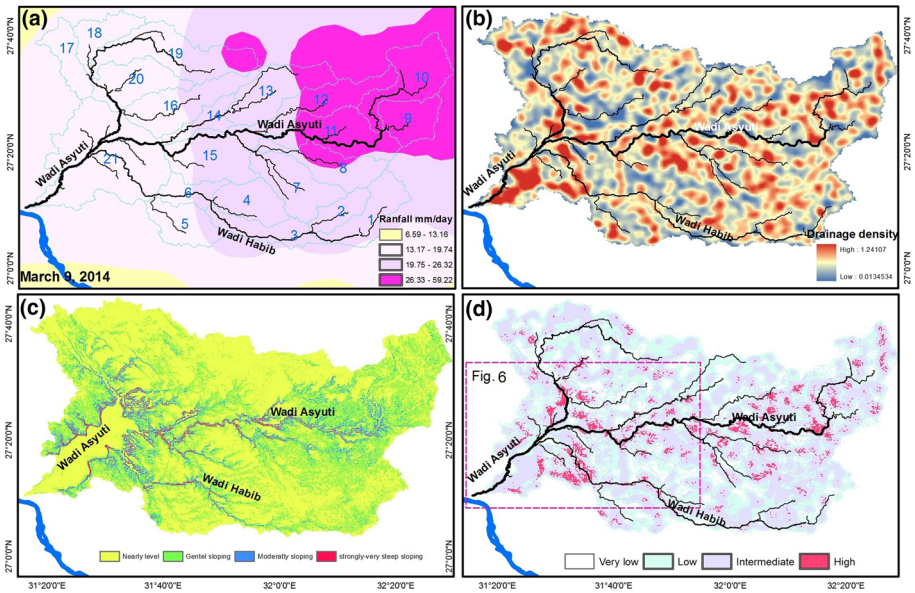

Fig. 5 Integrated data of Wadi Asyuti **a** rainfall anomaly map, **b** drainage density based on spatial distribution of stream networks, **c** classify of the slope of DEM, **d** combined slope and drainage density

with low rainfall. Despite the runoff starting from upstream taking longer travel time to reach the outlet, the excess of rainfall caused damage in the downstream portion in the direction of the water flow. The rainfall anomaly map (Fig. 5a) along with areas of high drainage density and steep slope (Fig. 5b) revealed areas prone to the possibility of flash flooding. The equivalent amount of rainfall in other areas, to the north, cannot initiate flash floods as other areas do not have steep slopes, relief, and low drainage density. Therefore, much of the hazard areas are located along the main stream of W. Asyuti (Fig. 6a, b).

Upland areas received high rainfall; however, the surface water flow through specific areas that represent the low land of the wadi course. These areas of flood plains are more desirable for human settlement and expansion (Alkema 2007; Mugisha 2015). However, it is temporarily inundated by water. In development countries, the new development areas have significantly increased, especially in the flood plain areas, due to rapidly increasing of population and urbanization. As much of the agricultural areas of the downstream of W. Asyuti were established by local farmers, the sites for farms, constructions, and infrastructures were selected without taking into consideration the flood aspects (Fig. 6b).

In order to understand the potential areas of hazard in the flood plain and the possibilities of sustainable development, we processed a Landsat-8 scene that was acquired on March 15, 2014, 6 days after significant storm (March 9, 2014). This also is to define the spatial extent of the flood that is of a crucial importance. The false color composite (bands 7, 5, 3 in R, G, and B) of Landsat-8 clearly highlighted the remnants of water bodies (blue color) along the main streams. Moreover, it highlighted wetted areas that preserve information on overland flow during runoff from a rain storm. This reflects that the main channel along the W. Asyuti accumulates the water in upstream of the catchments and drains it downstream (Fig. 6a, b). This observation confirmed the aforementioned results of rainfall anomalies on the eastern sub-basins that allowed water to flow in Wadi Asyuti

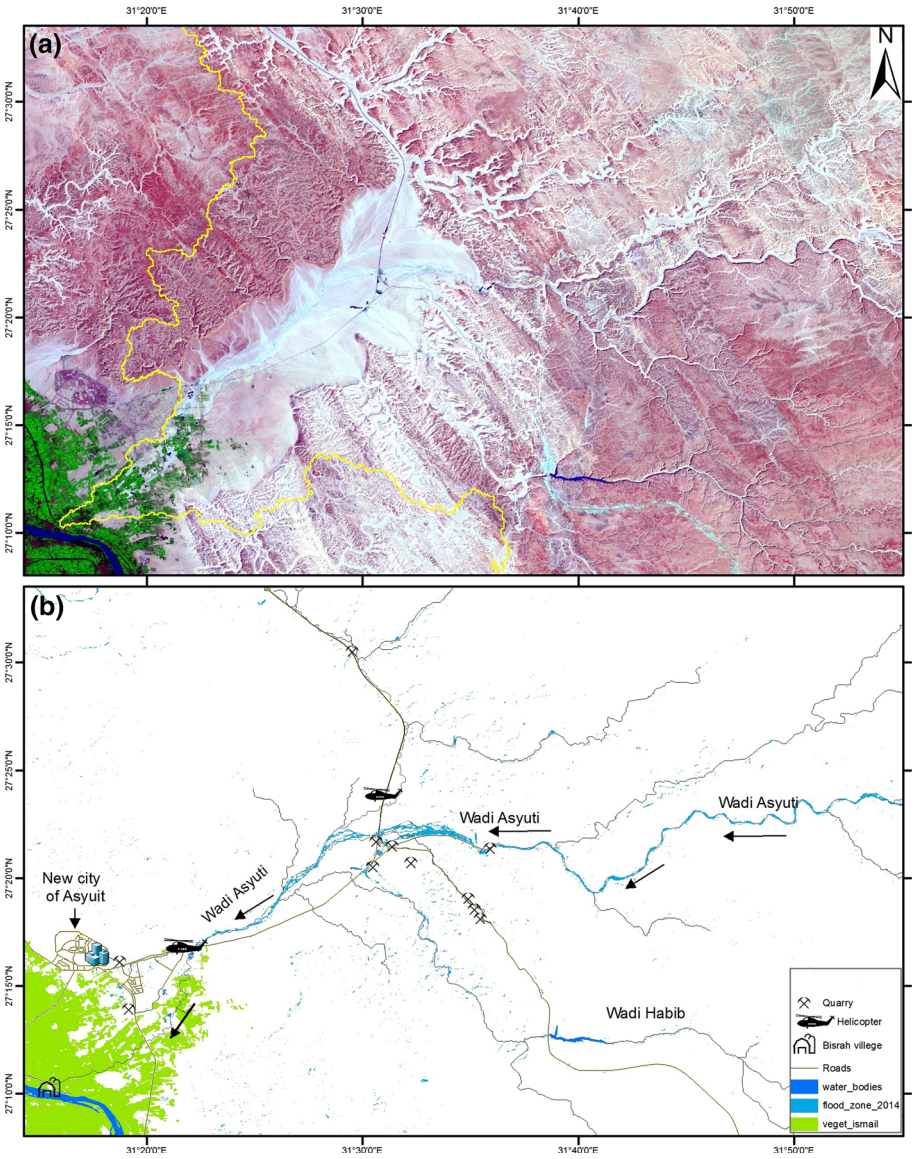

Fig. 6 **a** Landsat-8 acquired on March 15, 2014, 6 days later of the storm, revealing water bodies in blue and flood zone in *dark blue*, **b** extent of flooding zone (*light blue*) long W. Asyuti and its relationships to water bodies (*blue*), predicted streams (*black*), vegetated areas of the downstream and other land cover (quarries, airports)

main channel. This allowed collecting water through this stream to drain westerly where many farms are located (Fig. 6b). This scene also provided possibilities to calibrate and validate flash flood extents. The results of rainfall anomalies map coincidence with the observations of Landsat data and the physical characteristics of the basin. Runoff from sub-basins S9 and 10 takes more travel time and promotes water recharge through the below

alluvial aquifers. The runoff passes through >160 km to reach the downstream areas over a soil of permeable character.

Land-use mapping and planning is an important contribution to sustainable development. The extracted features (Fig. 6b) revealed the flood zone where many man-made structures and agricultural and industrial activities in the downstream are intersected by a flood plain. This coupled with increased accumulation of water in areas of higher activities that might create crises in low lands. In this image, a potential loss in a particular area of the downstream within a short period of time of the flash flood might be done in a future flooding event. One of a great importance is the new city of Asyut. It located in the outer zone of flooding, to the west; however, much of farms, commercial and industrial areas occur in real hazards. Therefore, structures such as dams, culverts, diversions, and artificial lakes (reservoir) might be preventing and protecting the social and economic activities from flooding. These approaches can be reduced the flood risk; however, it cannot guarantee an entire safety against flooding (Menzel and Kundzewicz 2003).

5 Summary and conclusions

This article focused on studying the morphometric characteristics of Wadi Asyuti in order to explain the physical characteristics and hydrologic conditions of the drainage system and to evaluate the flood potential. These objectives were implemented by using remotely sensed data including SRTM DEM, TRMM, and Landsat-8 that provided meaningful information about rainfall and flash flood hazards of the studied basin. Several factors were computed, including drainage characteristics, basin relief, texture, and geometry. The results show significant westerly flowing to the Nile basin as a result of the tilting of the plateau westward. This is responsible for transport of much meteoric water and sediment to the downstream area. The morphometric characteristics of the studied sub-basins were evaluated and examined to flash flood potentials. This was performed by using the potential contributing factors including bifurcation ratio, elongation ratio, form factor, circularity ratio, texture ratio, stream frequency, drainage density, infiltration number, basin relief, relief ratio, ruggedness number, and length of overland flow were integrated to highlight the extreme sub-basins to flash flood. Subsequently, we applied spatial distribution on the acquired rainfall data, slope, and stream density to highlight potential areas of hazard along the main stream. The proposed model was calibrated using Landsat-8 data that validated the rainfall data anomalies on the high relief and altitude of W. Asyuti. Moreover, it defined the extent of the flood zone along the main channel as the surface soil preserved evidence of the water content. Many strategies including structural features should be considered to reduce the flooding. The overall result revealed that using remotely sensed data provide significant information on the morphometric characteristics and highlighted potential areas of flooding and the extent of the flood zone. Although the new city of Asyut, east of the Nile Valley, is out of the flood zone, flood hazards represent an excessive threat to the people settlement and other activities in the downstream area.

Acknowledgments This research was supported by South Valley University. We thank Professor Farouk El-Baz, Director of the Center for Remote Sensing, Boston University and anonymous reviewers for their constructive comments, which helped us to improve the manuscript. And also, we would like to thank Dr. Karem Moubark and Samar Youssef, South Valley University.

References

Abdalla F, El Shamy I, Bamousa AO, Mansour A, Mohamed A, Tahoon M (2014) Flash floods and groundwater recharge potentials in arid land alluvial basins, southern Red Sea coast, Egypt. Int J Geosci 5:971–982

Abdel Ghaffar MK, Abdellatif AD, Azzam MK, Riad MH (2015) Watershed characteristic and potentiality of Wadi El-Arish, Sinai, Egypt. Int J Adv Remote Sens GIS 4(1):1070–1091

Abdelkareem M, El-Baz F (2015a) Mode of formation of the Nile Gorge in northern Egypt by DEM-SRTM data and GIS analysis. Geol J. doi:10.1002/gj.2687

Abdelkareem M, El-Baz F (2015b) Regional view of a trans-African drainage system. J Adv Res 6:433–439

Abdelkareem Mohamed, El-Baz Farouk (2015c) 2015 c. Analyses of optical images and radar data reveal structural features and predict groundwater accumulations in the central Eastern Desert of Egypt. Arab J Geosci 8:2653–2666

Abdelkareem M, Ghoneim E, El-Baz F, Askalany M (2012a) New insight on paleoriver development in the Nile basin of the eastern Sahara. J Afr Earth Sci 62:35–40

Abdelkareem M, El-Baz F, Askalany M, Akawy A, Ghoneim E (2012b) Groundwater prospect map of Egypt's Qena Valley using data fusion. Int J Images Data Fusion 3(2):169–189

Alkema (2004) RS and GIS applications in flood forecasting, p 3. http://ezproxy.utwente.nl:2980/papers/2004/n_p_conf/alkema_rs.pdf

Alkema D (2007) Simulating floods, On the application of a 2D-hydraluic model for flood hazard and risk assessment. International Institute for Geo-information Science and Earth Observation, Enschede, The Netherlands. http://www.itc.nl/library/papers_2007/phd/alkema.pdf

Alkema D, Cavallin A, De Amicis M (2001) Strategic application of flood modeling for infrastructure planning and impact assessment. In: Integrated water managment, proceeding of symposium held at Davis, California, April 2000 IAHS publication No. 272, pp 305–310

Bajabaa S, Masoud M, Al-Amri N (2014) Flash flood hazard mapping based on quantitative hydrology, geomorphology and GIS techniques (case study of Wadi Al Lith, Saudi Arabia). Arab J Geosci 7:2469–2481

Bangira T (2013) Mapping of flash flood potential areas in the Western Cape (South Africa) using remote sensing and in situe data. M.Sc, Enschede, Netherland

Biswas A, DasMajumdar D, Banerjee S (2014) Morphometry governs the dynamics of a drainage basin: analysis and implications. Geogr J. doi:10.1155/2014/927176

Chopra R, Dhiman RD, Sharma PK (2005) Morphometric analysis of sub-watersheds in Gurdaspur district, Punjab using remote sensing and GIS techniques. J Indian Soc Remote Sens 33(4):531–539

Chorley RJ, Morgan MA (1962) Comparison of morphometric features, UnakaMountains, Tennessee andNorth Carolina, and Dartmoor, England. Geol Soc Am Bull 73(1):17–34

Chorley RJ, Donald Malm EG, Pogorzelski HA (1957) A new standard for estimating drainage basin shape. Am J Sci 255:138–141

Davis JC (1975) Statics and data analysis in geology. Wiley, New York

Dawod GM, Mirza MN, Al-Ghamdi KA (2011) GIS-Based Spatial Mapping of Flash Flood Hazard in Makkah City, Saudi Arabis. J Geogr Inf Syst 3:225–231

El-Bastawesy M, White K, Nasr A (2009) Integration of remote sensing and GIS for modeling flash flood in Wadi Hudain Catchment, Egypt. Hydrol Process 23(9):1359–1368

Faniran A (1968) The index of drainage intensity—a provisional new drainage factor. Aust J Sci 31:328–330

Gardiner V (1990) Drainage basin morphometry. In: Goudie A (ed) Geomorphological techniques. Unwin Hyman, London, pp 71–81

Gregory KJ, Walling DE (1973) Drainage basin form and process: a geomorphological approach. Edward Arnold, London, p 456

Grohmann CH, Riccomini C, Alves FM (2007) SRTM-based morphotectonic analysis of the Pocos de Caldas Alkaline Massif, Southeastern Brazil. Comput Geosci 33:10–19

Horton RE (1932) Drainage-basin characteristics. Trans Am Geophys Union 13:350–361

Horton RE (1945) Erosional development of streams and their drainage basins. Bull Geol Soc Am 56:275–370

Kale VS, Guptha A (2001) Introduction to geomorphology. Orient Longman Ltd, Hyderabad

Lyew-Ayee P, Viles HA, Tucker GE (2007) The use of GISbased digital morphometric techniques in the study of cockpit karst. Earth Surf Process Landf 32(2):165–179

Marchi L, Borga M, Preciso E, Gaume E (2010) Characterisation of selected extreme flash floods in Europe and implications for flood risk management. J Hydrol 394(1–2):118–133

Melton MA (1957) An analysis of the relations among elements of climate, surface properties and geomorphology, Project NR 389042, Tech. Rep. 11, Columbia University

Menzel L, Kundzewicz ZW (2003) Non structural flood protection-a challenge. International conference, Towards natural flood reduction stratigies, Warsaw, 6–13 September, pp 1–5
Miller VC (1953) A quantitative geomorphic study of drainage basin characteristics in the Clinch Mountain area, Varginia and Tennessee, Project NR 389042, Tech. Rept. 3., Columbia University, Department of Geology, ONR, Geography Branch, New York
Mugisha F (2015) Modeling and assessment of urban flood hazards based on end-user requirements. Kigali-Rwanda. M.Sc, Enschede, The Netherland
Nageswara Rao K, Swarna Latha P, Arun Kumar P, Hari Krishna M (2010) Morphometric analysis of Gostani river basin in Andhra Pradesh State, India using spatial information technology. Int J Geomat Geosci 1(2):179–187
O'Callaghan JF, Mark DM (1984) The extraction of drainage networks from digital elevation data. Comput Vis Gr Image Process 28:323–344
Patton PC (1988) Drainage basin morphometry and floods. In: Baker VR et al (eds) Flood geomorphology. Wiley, New York, pp 51–65
Patton PC, Baker VR (1976) Morphometry and floods to small drainage basins subject to diverse hydrographic controls. Water Resour Res 12(5):941–952
Rudraiah M, Govindaiah S, Vittala SS (2008) Morphometry using remote sensing and GIS techniques in the sub-basins of Kagna river basin, Gulburga district, Karnataka, India. J Indian Soc Remote Sens 36(4):351–360
Schumn SA (1956) Evaluation of drainage systems and slopes in badlands at Perth Amboy, New Jersy. Bull Geol Soc Am 67:597–646
Şen Z, Khiyami AH, Al-Harthy SG, Al-Ammawi FA, Al-Balkhi AB, Al-Zahrani MI, Al-Hawsawy HM (2012) Flash flood inundation map preparation for wadis in arid regions. Arab J Geosci. doi:10.1007/s12517-012-0614-6
Singh S, Singh MC (1997) Morphometric analysis of Kanhar river basin. Natl Geogr J India 43(1):31–43
Smith KG (1950) Standards for grading texture of erosional topography. Am J Sci 248:655–668
Somashekar RK, Ravikumar P (2011) Runoff estimation and morphometric analysis for Hesaraghatta watershed, a remote sensing and GIS approach. J Indian Soc Remote Sens 39(1):95–106
Strahler AN (1952) Hypsometric analysis of erosional topography. Bull Geol Soc Am 63:1117–1142
Strahler AN (1957) Quantitative analysis of watershed geomorphology. Trans. Amer. Geophys. Union. 38:913–920
Strahler AN (1964) Quantitative geomorphology of drainage basins and channel networks. In: Chow VT (ed) Handbook of applied hydrology, McGraw Hill Book Company, New York, Section 4II
Syvitski PMJ, Kettner JA, Overeem I, Hutton WHE, Hannon TM, Brakenridge RG, Day J, Vorosmarty C, Saito Y, Giosan I, Nicholls JR (2009) Sinking deltas due to human activities. Nat Geosci 2:681–686
Waikar ML, Nilawar AP (2014) Morphometric analysis of a drainage basin using geographic information system: a case study. Int J Multidiscip Curr Res 2:179–184
Waugh D (1995) Geography, an integrated approach. Nelson, New York
Withanage NS, Dayawansa NDK, De Silva RP (2014) Morphometric analysis of the Gal Oya river Basin using spatial data derived from GIS. Trop Agric Res 26(1):175–188
Youssef A, Pradhan B, Hassan A (2010) Flash flood hazards assessment, management, and mitigation, in Wadi Ady, Muscat area, Sultanate of Oman, a GIS& remote sensing approach. Egypt J Remote Sens Space Sci 12(1):71–86
Youssef AF (2008) The impact of north west active fault system on the recharge of the quaternary aquifer system around Nile Valley: case study Wadi El-Assuity, Eastern Desert, Egypt. Eur Water 21(22):41–55